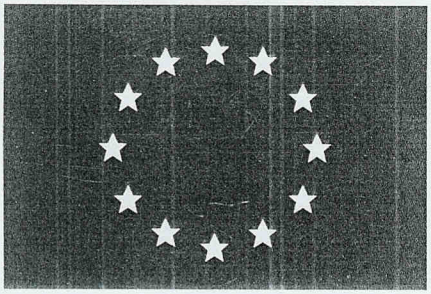

EUROPEAN COMMISSION

Gefördert vom

bmb+f

Bundesministerium für
Bildung, Wissenschaft,
Forschung und Technologie

Air pollution research report 56

Polar stratospheric ozone

Proceedings
of the
third European workshop
18 to 22 September 1995
Schliersee, Bavaria, Germany

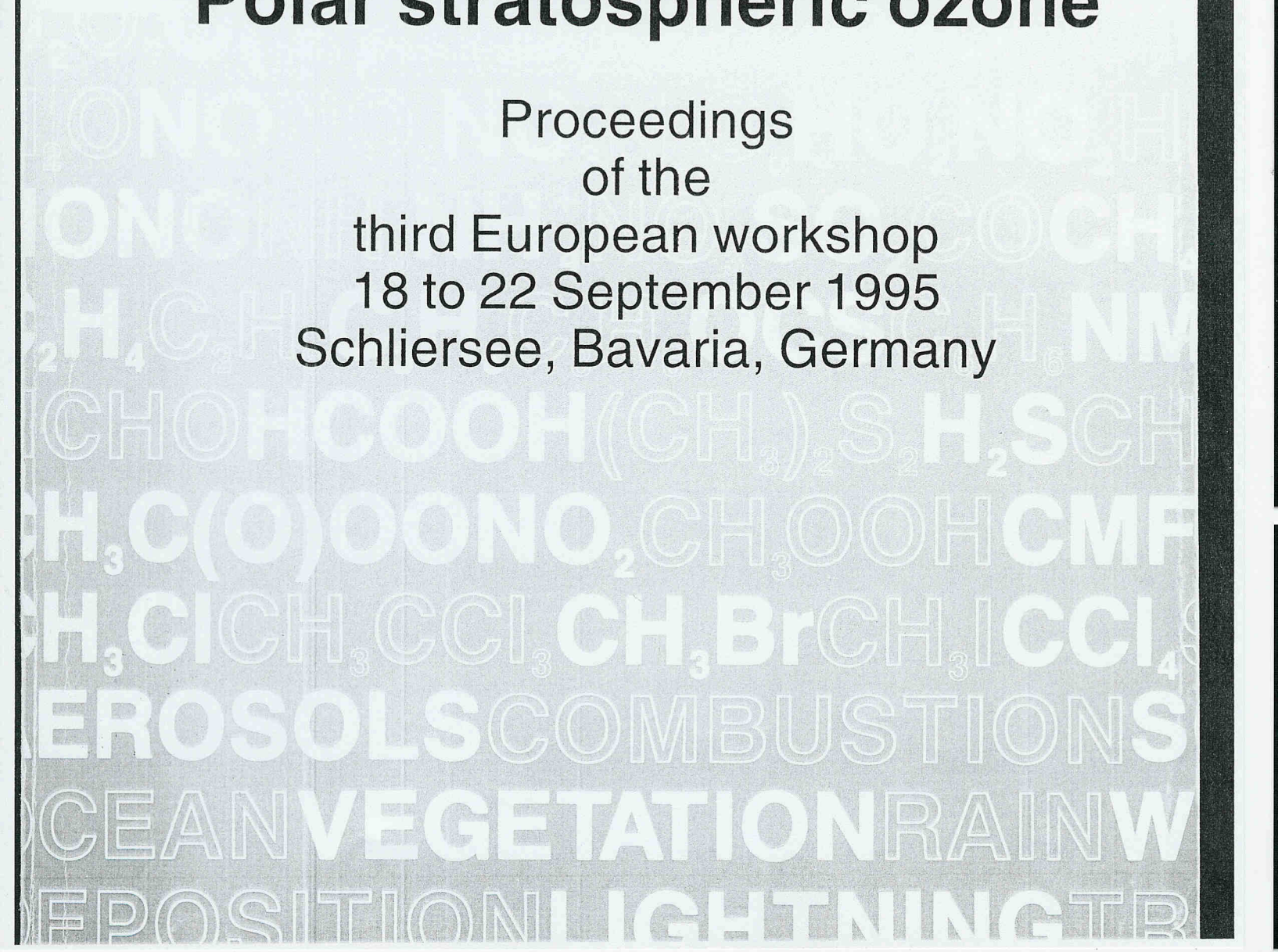

Presented at the Third European Symposium on Polar Stratospheric Ozone Research (Schliersee, Germany, 18-22 September 1995)

RESULTS OF A TRAJECTORY BOX MODEL SIMULATING THE SIZE DISTRIBUTION EVOLUTION OF STRATOSPHERIC PARTICLES (H_2SO_4/H_2O and H_2SO_4/HNO3/H2O SOLUTIONS). A CASE STUDY DURING SESAME.

V. Rizi, G. Redaelli and G. Visconti
Dipartimento di Fisica, Università Degli Studi - L'Aquila, Italy.
F. Masci
Istituto Nazionale di Geofisica, L'Aquila, Italy.
I. Ivanova
Institute of Electronics, Bulgarian Academy of Science, Sofia, Bulgaria.
C. Wedekind, F. Immler, B. Mielke, P. Rairoux, B. Stein, L. Woste
Freie Universitat Berlin, Berlin, Germany.
M. Del Guasta, M. Morandi, L. Stefanutti
IROE/CNR, Firenze, Italy
R. Matthey, V. Mitev
Observatorie Cantonal Neuchatel, Neuchatel, Swizerland
M. Douard, J. P. Wolf
Universitè Lyon, Villeurbanne, France
E. Kyro, R. Kivi
Finnish Meteorological Institute, Sodankyla, Finland

Introduction.

A revised interpretation of ER-2 polar stratospheric cloud (PSC) observations during AASE I (1989) and AAOE (1987) (Tabazadeh et al., 1995) suggests a picture of the PSC formations which evidences the importance of the air mass thermal histories. A series of ER-2 measurements are consistent with the thermodynamical properties of the liquid $H_2SO_4/HNO_3/H_2O$ solution particles, but the data collected in other flights are in agreement with the possible formation of amorphous solid solutions of HNO_3 and H_2O through a peculiar cooling/heating cycle below the solid sulfuric acid tetrahydrate (SAT) melting temperatures and above the water ice saturation temperatures (frost point). During this cycle the liquid H_2SO_4 stratospheric aerosols may undergo a phase transition to SAT particles, required for the growing of solid nitric acid hydrates.
On the other hand Koop et al., (1995) report laboratory experiments which show that $H_2SO_4/HNO_3/H_2O$ liquid particles never freeze under stratospheric conditions for temperatures higher than the frost point, despite the change in composition due to the HNO_3 uptake when cooling. In addition, when solid particles are heated, they start to become liquid at the SAT melting point.
Then the analysis of any PSC data should start from air mass trajectory studies, and some thermodynamical criteria could be used to infer the physical state (liquid or solid) of the sampled particles.
We use a trajectory box model to study the microphysical properties of stratospheric clouds observed during SESAME by the MOANA (Measurements and modelling of Ozone and Aerosols in the Northern Atmosphere) lidar at Sodankyla (SF). Our models treats the gas to particle conversion of H_2SO_4, HNO_3, H_2O and the microphysics of Aitken particles (ATK), H_2SO_4/H_2O (WS) and $H_2SO_4/HNO_3/H_2O$ (WSN) solution droplets; H_2SO_4 - nH_2O (SA) and HNO_3 - nH2O (NA) solid hydrates particles are also taken into account.
To analyze the MOANA observations, within a prescribed air mass thermal history, we adopt a simple criteria which states that the particles should be liquid just after having performed temperatures above the SAT melting point, while they are solid if the water ice saturation temperatures are reached.
The model simulations along the air mass trajectories reaching the lidar site during the observations are in agreement with the aerosol size distribution optically retrieved by the MOANA multiwavelength lidar (Masci et al., 1995).

Model description.

The aim of our Aerosol Model (AM) is to simulate the dynamical evolution of the aerosol size distributions in the stratosphere. Our box AM represents an air mass following a thermal history prescribed by a calculated isentropic back-trajectory. The aerosol physical processes accounted in AM include:
- heteromolecular homogeneous and heterogeneous nucleation of binary WS solution over ATK particles, of NA and ice over NA and SA particles;

- homogeneous and heterogeneous freezing/melting nucleation of solid NA and SA from WS and WSN liquid solutions;
- diffusional condensation/evaporation of H_2SO_4, HNO_3 and H_2O to/from WS and WSN liquid particles and to/from SA and NA solid particles;
- coagulation.

The numerical algorithms simulating the physical processes have been developed on the basis of works of Toon et al, 1988, and Larsen, 1991; in addition the core return mechanism in the evaporation process is exactly treated making AM suitable to realistic air mass thermal histories (Rizi et al., 1995). This formulation of an aerosol model has important limitations due to the poor understanding or to the simplified treatment of some physical processes (i.e. heteromolecular nucleation and freezing/melting mechanisms) and to the lack of some thermodynamical data (i.e. vapour pressure of the relevant gases over the liquid or solid solutions which likely constitute the stratospheric aerosols and the surface energies of these solutions for the pressure and temperature ranges of the stratosphere). Our AM includes the most recent data and results (i.e. Zhao et al., 1995, Luo et al., 1995, MacKenzie et al., 1995 and cited references).

January 19, 1995 polar stratospheric clouds.

To simulate the PSC detected with MOANA lidar on January 19, 1995 (Masci et al., 1995) we have made an analysis of the different air masses reaching Sodankyla during the lidar measurements: the air mass thermal history at 475K potential temperature level (about 20 km) arriving over Sodankyla at 14:00 GMT is representative of the detected PSC and is shown in Fig.1.

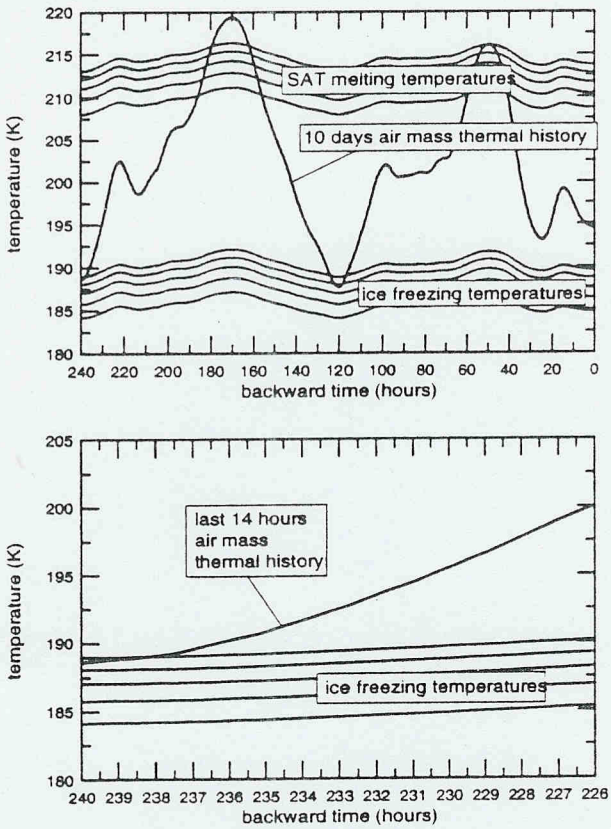

Figure 1. 475 potential temperature levels air mass thermal history along the backward trajectories reaching Sodankyla (SF) at 14:00 GMT during the lidar sampling on January 19, 1995. The SAT melting temperatures (Zhang et al., 1993) and the water ice saturation temperatures are shown for different water vapour contents of the stratosphere (from 3ppmv, lower temperatures to 7 ppmv, higher temperatures).

50 hours before being sampled the air mass is heated up to about 220K, well above the SAT melting temperatures, a cooling follows and the temperature goes down to 188K over the lidar site, but above the ice freezing temperatures. Then the increase in the aerosol backscattering ratio should indicate an increase in the typical radii of the sampled particles due to the condensation from gas phase of nitric, sulfuric acid and water in liquid supercooled ternary solution aerosols. This physical state of the particles is in agreement with the MOANA lidar observations, because no depolarization signal has been measured (Masci et al., 1995), suggesting that the PSC aerosols are likely spherical (liquid) droplets.

We have generated a background aerosol field (WS solution droplets) in the Arctic stratosphere (constant temperature profile, T=220K) running the model until a steady state has been reached, and we have taken the size distribution of such aerosols and the ambient gas concentrations as initial state of the air mass sampled by the lidar after following the isentropic trajectory of Fig.1.

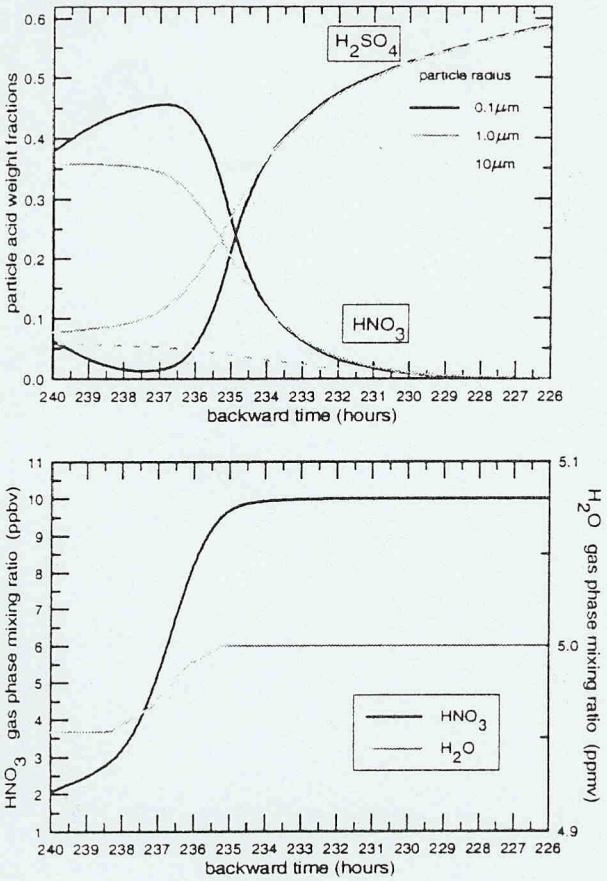

Figure 2. *The simulated evolution of HNO_3 and H_2SO_4 weight fractions in different WSN particles and of HNO_3 and H_2O gas phase along the air mass trajectories reaching MOANA lidar site at 14:00 GMT of January 19, 1995.*

The initial values of H_2O and HNO_3 concentrations are 5 ppmv and 10 ppbv respectively, the initial size distribution of the WS aerosols is a well fitted by a log-normal distribution with median radius r_o=0.075μm and geometrical width σ=1.75.

The results of AM simulations at 475K potential temperature level are shown in Fig.2 for the last 14 hours of the air mass thermal history. During the growing of the WSN particles, HNO_3 and H_2O molecules are removed from the gas phase, the temporal behaviour of the acid weight fractions in the particles is strictly connected to the particle radius due to size dependence of the thermal and kinetic effects in the diffusional condensation processes. Then, according to AM the lidar has detected WSN liquid solution aerosols formed in the sampled air masses few hours before reaching Sodankyla.

The aerosol size distributions predicted at the end of the backward trajectories are shown in Fig.3. The condensation of HNO_3 , H_2O and H_2SO_4 when the air mass temperature has cooled down increases the number density of the particles at larger radii, a second mode in the size distribution appears at about 0.4μm. The aerosols with radius between 0.1μm and 1.0μm have the highest weight fraction of nitric acid, below this range the Kelvin effect prevents the condensation of HNO_3 molecules, and above the kinetic and thermal resistance to the diffusional condensation processes of nitric acid makes the particles more rich of H_2O and H_2SO_4.

These results are comparable with the size distribution estimated directly from the lidar observations (Masci et al., 1995). The backscattering ratios at the MOANA lidar wavelength are well fitted by a refractive index near to those of liquid water particles (i.e. 1.35 at λ = 532nm) and an equivalent log-normal size distribution with median radius r_o = 0.50 ± 0.10 μm, geometrical dispersion σ = 1.35 ± 0.10 and total particle density N_o = (5.0 ± 2.0) 10^6 particles m^{-3} .

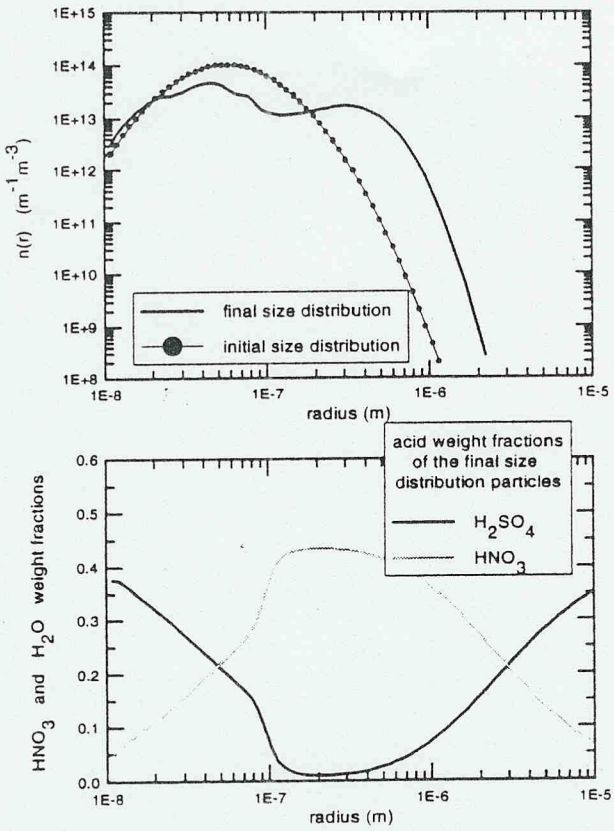

Figure 3. The AM simulated particle size distribution over MOANA lidar, the HNO_3 and H_2SO_4 weight fraction are shown as functions of the particle radius.

The comparison between the lidar results and the AM simulation should account that the lidar backscattering ratio is mainly sensitive to a particular radius range, which is connected to the lidar wavelength and to the Mie scattering features. Then we could compare the quantities:

$$S_{OPT}(r) = dr\,\pi\,r^2\,n_{OPT}(r)$$

$$S_{AM}(r) = dr\,\pi\,r^2\,Q_{bck}(r)\,n_{AM}(r)$$

where r is the particle radius, Q_{bck} (r) is the Mie backscattering efficiency of the sampled particles (calculated averaging the efficiencies at the different wavelengths), n_{OPT} (r)dr and n_{AM}(r)dr are respectively the size distributions retrieved from the lidar measurements and simulated by AM. In such a way we skip the lidar optical filtering of the particles, with a direct comparison between the effective cross section size distributions. The results are shown in Fig.4.

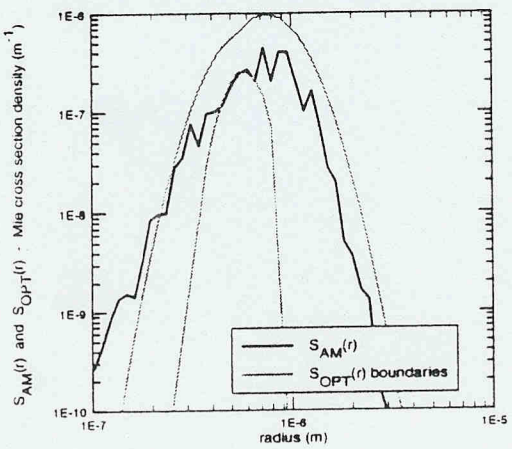

Figure 4. Comparison between the Mie cross section densities (see text). The black solid line refers to AM results, and the gray solid lines represent the upper and the lower limits of the optically retrieved Mie cross section density.

References

Koop et al., Do stratospheric aerosol droplets freeze above the ice frost point?, *Geophys. Res. Lett., 22,* 917-920, 1995.

Larsen N., Polar stratospheric clouds: a microphysical simulation model, *Danish meteor. Inst. Rep., 91-2,* 1991.

Luo et al., Vapour pressure of $H_2SO_4/HNO_3/HCl/HBr/H_2O$ solutions to low stratospheric temperatures, *Geophys. Res. Lett., 22,* 247-250, 1995.

MacKenzie et al., On the theories of type 1 polar stratospheric cloud formation, *J. Geophys. Res., 100,* 11275-11288, 1995.

Masci et al., Polar stratospheric clouds observations at Sodankyla (SF), *this issue,* 1995.

Rizi et al., Numerical setups for an Aerosol Model simulating the evolution of stratospheric aerosol size distributions, *in preparation,* 1995.

Tabazadeh et al., Freezing behavior of stratospheric sulfate aerosols inferred from trajectory studies, *Geophys. Res. Lett., 22,* 1725-1728, 1995.

Toon et al., A multidimensional model for aerosols: description of computational analogs, *J. Atmos. Sci., 45,* 2123-2143, 1988.

Zhang et al., Physical chemistry of the H_2SO_4/H_2O binary system at low temperatures: Stratospheric implications, *J. Phys. Chem., 97,* 7351, 1993.

Zhao et al, A model simulation of Pinatubo volcanic aerosols in the stratosphere, *J. Geophys. Res., 100,* 7315-7328, 1995.

References

Koop et al., Do stratospheric aerosol droplets freeze above the ice frost point?, *Geophys. Res. Lett., 22,* 917-920, 1995.

Larsen N., Polar stratospheric clouds: a microphysical simulation model, *Danish meteor. Inst. Rep., 91-2,* 1991.

Luo et al., Vapour pressure of $H_2SO_4/HNO_3/HCl/HBr/H_2O$ solutions to low stratospheric temperatures, *Geophys. Res. Lett., 22,* 247-250, 1995.

MacKenzie et al., On the theories of type 1 polar stratospheric cloud formation, *J. Geophys. Res., 100,* 11275-11288, 1995.

Masci et al., Polar stratospheric clouds observations at Sodankyla (SF), *this issue,* 1995.

Rizi et al., Numerical setups for an Aerosol Model simulating the evolution of stratospheric aerosol size distributions, *in preparation,* 1995.

Tabazadeh et al., Freezing behavior of stratospheric sulfate aerosols inferred from trajectory studies, *Geophys. Res. Lett., 22,* 1725-1728, 1995.

Toon et al., A multidimensional model for aerosols: description of computational analogs, *J. Atmos. Sci., 45,* 2123-2143, 1988.

Zhang et al., Physical chemistry of the H_2SO_4/H_2O binary system at low temperatures: Stratospheric implications, *J. Phys. Chem., 97,* 7351, 1993.

Zhao et al, A model simulation of Pinatubo volcanic aerosols in the stratosphere, *J. Geophys. Res., 100,* 7315-7328, 1995.